Rational Design, Synthesis and In Vitro Activity of Heterocyclic Gamma-Butyrobetaines as Potential Carnitine Acetyltransferase Inhibitors

Savina Stoyanova and Milen G. Bogdanov *

Posted Date: 16 December 2024

doi: 10.20944/preprints202412.1211.v1

Keywords: Carnitine acyltransferase; L-carnitine; fatty acids oxidations; enzyme inhibition

Article

Rational Design, Synthesis and In Vitro Activity of Heterocyclic Gamma-Butyrobetaines as Potential Carnitine Acetyltransferase Inhibitors

Savina Stoyanova and Milen G. Bogdanov *

Faculty of Chemistry and Pharmacy, Sofia University St. Kl. Ohridski, 1, Jammes Bourchier blvd., 1164 Sofia, Bulgaria

* Correspondence: mbogdanov@chem.uni-sofia.bg

Abstract: This study examined heterocyclic gamma-butyrobetaine (GBB) analogs as metabolic modulators through rational design, docking, synthesis, and in vitro analyses. The compounds inhibited carnitine acetyltransferase (CAT) and possibly other enzymes in the carnitine transferase family, showing inhibitory potential in the low millimolar range (IC_{50} = 2.24–43.6 mM), with some more active than the well-known drug Meldonium (IC_{50} = 11.39 mM). Key findings include that bulky and hydrophobic substituent at the gamma-position enhances inhibition, while esterification and increased polarity reduce it. The most active compound was identified as a reversible competitive inhibitor of CAT, with a K_i value of 3.5 mM, similar to Meldonium's K_i of 1.63 mM. These results indicate that heterocyclic GBB analogs are potential candidates for regulating metabolic processes and for treating conditions such as ischemic diseases, diabetes, and certain cancers.

Keywords: Carnitine acyltransferase; L-carnitine; fatty acids oxidations; enzyme inhibition.

1. Introduction

Carnitine acyltransferases (CT) constitute a family of essential mammalian cellular enzymes crucial for bioenergetic processes in human and animal cells [1–4]. Their primary function pertains to the oxidation of fatty acids (FAO) within the mitochondria, which represents a main energy source alongside glucose oxidation. However, the transport of FA from the cytosol into the mitochondria, where FAO occurs, requires a specific mechanism because FA cannot diffuse directly into the mitochondria [5]. This transport mechanism involves at least three distinct enzymatic reactions known as the carnitine shuttle, with the CT managing the initial and rate-limiting component by facilitating the reversible transfer of fatty-acid-derived acyl groups between coenzyme A (CoA) and the amino acid L-carnitine [6,7].

CT family consists of three distinct subsets: carnitine acetyltransferase (CAT), carnitine octanoyltransferase (COT), and carnitine palmitoyltransferase (CPT) [8–11]. These subsets are responsible for the translocation of FA with varying chain lengths between cellular compartments, specifically the cytosol and the mitochondria. The CAT subset is responsible for short-chain fatty acids, such as acetate and propionate, and is localized within the mitochondria, endoplasmic reticulum, and cytoplasmic peroxisomes [12]. The COT subset is involved in processing medium-chain fatty acids, including octanoate and heptanoate, and is predominantly situated in the cytoplasmic peroxisomes. Lastly, the CPT subset manages long-chain fatty acids, such as palmitate and stearate, and is primarily located in the inner and outer mitochondrial compartments. Despite the above differences in function and localization, these subsets share significant structural similarities, and compounds proven to affect one subset are often found to be active against the others [8,13].

 doi:10.20944/preprints202412.1211.v1

Notably, while the prevailing medical hypothesis supports the notion that increased rates of FAO are advantageous, early studies from the 1960s have contested this perspective [14]. Given this data and the crucial significance of the CT enzyme family in FAO, extensive research to elucidate their structure, function, and potential for therapeutic intervention have been undertaken over the past few decades. As a result, CT has emerged as promising targets for addressing various chronic conditions, including cardiovascular disease [15–17], diabetes [18–24], renal [25] and hepatic [26] conditions, mental [27] and neurodegenerative disorders [28–30], and viral pulmonary pathology [31], to name just a few. In addition, in contrast to the widely held belief that cancer cells depend on glucose for proliferation and metastasis, recent evidence has challenged this dogma by highlighting the potential role of excessive FAO in driving the cancerization of normal tissues and the metastatic process [32]. Consequently, FAO inhibition has also emerged as a highly promising therapeutic strategy for various cancer types, devoid of known resistance mechanisms characteristic of conventional cytotoxic chemotherapy [33–41]. All this led to the development of small molecule compounds that function as FAO inhibitors by targeting specific subsets of the CT enzyme family, e.g., Meldonium, Etomoxir, Teglicar, Perhexillene [32].

The two most extensively researched examples of CT inhibitors are Meldonium [42–44] and Etomoxir [45,46]. The primary proposed mechanism of action for Meldonium (marketed as Mildronate®, an approved drug for the treatment of heart ischemia) involves targeting *de novo* L-carnitine biosynthesis by inhibiting the enzyme gamma-butyrobetaine dioxygenase (BBOX) [47,48]. Additional research has also revealed its potential as an inhibitor of organic cation/carnitine transporter OCTN2 and CAT [44,49]. In contrast, Etomoxir (a drug candidate failed Phase II clinical trial) primarily targets the CPT subset of enzymes while also exhibiting inhibitory activity against CAT and COT [50–52]. Despite their demonstrated therapeutic potential, some approved drugs (e.g., Meldonium) exhibit a number of drawbacks, including a relatively weak affinity for the CT [44], or toxicity (e.g., Etomoxir) by evoking oxidative stress, hepatoxicity, inhibition of electron transport chain complexes, etc. when used in clinically relevant concentrations [39,53,54]. Hence, the development of novel CT inhibitors with amplified potency and reduced toxicity bears considerable scientific and clinical potential [32].

Based on the above discussion, we have designed this study to demonstrate that heterocyclic gamma-butyrobetaine (GBB) analogs have the potential to serve as metabolic modulators. This potential is due to their initially hypothesized inhibitory activity against carnitine acetyltransferase and possibly other enzymes in the carnitine transferase family. Our investigation includes rational design, molecular docking, synthesis, and in vitro assay methodologies.

2. Results and Discussion

2.1. Rational Design

Understanding the active site structure and specific enzyme-substrate and enzyme-inhibitor/activator interactions is imperative in developing potent enzyme inhibitors or activators. The data presented in Table 1 [8,9,55], derived from isolated CATs from human, mouse, and pigeon sources [9,12,56], reveal a shared amino acid sequence in the L-carnitine binding active sites, despite variances in the polypeptide chains' primary structures. Notably, this structural similarity extends to other enzymes within the CT family, such as COT, CPT1, and CPT2 [13,55]; therefore, one can confidently extrapolate the insights gained from one enzyme to the others.

Table 1. Fragments of the amino acid (AA) sequences of human, mouse, pigeon and rat CT, showing those AA, directly involved in the binding of L-carnitine.

	AA sequence	AA position	AA sequence	AA position	AA sequence	AA position
Human (CAT)[8]	T**Y**ESASL**R**MFHLGR**T**D	430-445	GEAFD**R**HLLGL	492-502	DCVMF**F**GP**V**VP	540-550
Mouse (CAT)[8]	T**Y**ESASL**R**MFHLGR**T**D	452-467	GEAFD**R**HLLGL	514-524	DCVMF**F**GP**V**VP	562-572
Mouse (CAT)[57]	T**Y**ESASL**R**MFHLGR**T**D	422-437	GEAFD**R**HLLGL	484-494	DCVMF**F**GP**V**VP	532-542
Pigeon (CAT)[55]	T**Y**ESASL**R**MFRLGR**T**D	453-468	GNAID**R**HLLGL	514-524	DCVMC**F**GP**V**VP	562-572
Human (COT)[8]	C**Y**ETAMT**R**HFYHGR**T**E	438-453	GKGFD**R**HLLGL	500-510	GYLRVQGV**V**VP	548-558

 doi:10.20944/preprints202412.1211.v1

Human (CPT1)[8]	TYEASMTRLFREGRTE	588-603	GSGIDRHLFCL	650-660	SSGGGFGPVAP	706-716
Human (CPT2)[13]	TYESCSTAAFKHGRTE	485-500	GQGFDRHLFAL	549-559	VNLGGFAPVVS	598-608
Rat (CPT2)[57]	TYESCSTAAFKHGRTE	454-469	GQGFDRHLFAL	518-528	VSLGGFAPVVP	566-576

A range of interactions, encompassing hydrogen bonds, hydrophobic interactions, and π-cation interactions, as depicted in Figure 1, determines the efficiency and stability of the L-carnitine–CAT enzyme-substrate complex. The major role plays histidine, which dictates the acylation of the substrate—His322 for human-isolated enzymes, or His314 for those derived from mice (Mus Musculus). Specifically, the hydrogen bonding of the hydroxyl group of L-carnitine with the nitrogen atom (N3) of the imidazolium ring of histidine, followed by complete deprotonation, plays a pivotal role in shaping the stereospecificity of the reaction. In addition, the carboxyl group of the substrate forms hydrogen bonds with specific amino acids (Tyr431, Arg497, and Thr444 for human enzymes, and Tyr423, Arg489, and Thr436 for mouse-derived enzymes). Furthermore, the quaternary nitrogen atom of the substrate is positioned within a hydrophobic pocket, with its positive charge being partly stabilized by interactions with valine and phenylalanine (Val548 and Phe545 for human enzymes, and Val540 and Phe536 for mouse enzymes).

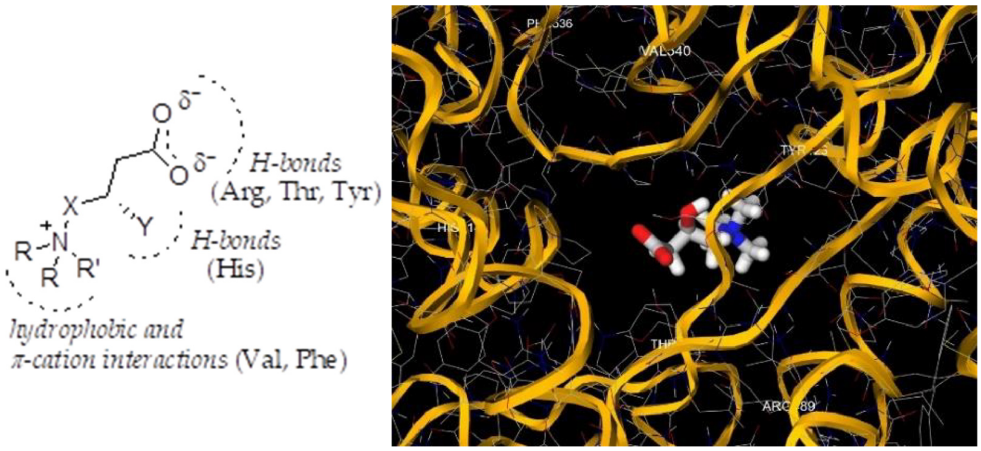

Figure 1. Left—Schematic representation of the specific interactions in enzyme-substrate complex of: 1) L-carnitine (natural substrate): X = CH_2; Y = OH; R = R = R′ = methyl; 2) Meldonium (approved drug): X = NH; Y = H; R = R = R′ = methyl; 3) MeGBB (3rd phase cl. trials): X = CH_2; Y = H; R = R = methyl; R′ = ethyl; 4) heterocyclic GBB: X = CH_2; Y = H; R = R = cycle; R′ = methyl; 5) heteroaromatic GBB: X = CH_2; Y = H; R = R = R′ = cycle; right—L-carnitine and depicted amino acids that are responsible for the specific substrate-enzyme interactions. View through the active site "tunnel".

Based on the above analysis, we hypothesized that incorporating a heterocyclic ring as a substituent in the gamma-position of butanoic acid could be a prerequisite for reinforcing the hydrophobic and π-cation interactions within the enzyme's hydrophobic pocket (see Figure 1). This reinforcement is expected to result in stronger inhibition of CAT when compared to Meldonium, as an example, which lack ring substituents containing the quaternary nitrogen atom (see Figure 2). Furthermore, introducing an aromatic substituent is considered necessary to facilitate π-π interactions, further augmenting the affinity of these analogs for the enzyme's active site.

To investigate this hypothesis, we initiated theoretical studies (molecular docking) to compare the binding affinity of hypothetical CAT inhibitors containing heterocyclic substituents with that of the natural substrate L-carnitine and the inhibitors Meldonium and 4-(ethyldimethylammonio)butanoate (MeGBB—a drug candidate in phase III of clinical trials). The study utilized the freely available online platform Mcule (http://mcule.com) and leveraged the structures for CAT isolated from mouse (Mus musculus, PDB identifier: 1ndi) and CPT2 isolated from rat (Rattus norvegicus, PDB identifier: 2fw3). Candidate cyclic aliphatic tertiary amines including *N*-methylpyrrolidine, *N*-methylpiperidine, and *N*-methylmorpholine were chosen, along with aromatic representatives such as *N*-methylimidazole, pyridine, *N*,*N*-dimethyl-4-aminopyridine, quinoline,

 doi:10.20944/preprints202412.1211.v1

and isoquinoline. Additionally, the bromides of the corresponding ethyl esters of the quaternary gamma-butyrobetaines were included to evaluate the impact of hydrogen bonding. The structural features of the studied compounds and the resultant findings are concisely presented in Figure 2, where a lower absolute value denotes a higher binding affinity of the inhibitor to the active site.

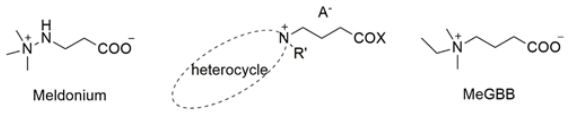

R	R'	Abbr.	X	A⁻	CAT	CPT2
L-carnitine					-4.3	-4.5
Meldonium					-3.9	-4.4
	$-CH_3$	MeGBB	O^-	-	-4.0	-4.7
	$-CH_3$	MeGBB-ester	-OEt	Br^-	-4.0	-5.0
	$-CH_3$	pyrr-GBB (**1**)	O^-	-	-4.5	-5.4
	$-CH_3$	**1** - ester	-OEt	Br^-	-4.5	-5.4
	$-CH_3$	pip-GBB (**2**)	O^-	-	-5.0	-5.6
	$-CH_3$	**2** - ester	-OEt	Br^-	-5.1	-5.5
	$-CH_3$	morph-GBB (**3**)	O^-	-	-4.7	-5.2
	$-CH_3$	**3** - ester	-OEt	Br^-	-4.6	-5.6
	-	mim-GBB (**4**)	O^-	-	-4.3	-5.3
	-	**4** - ester	-OEt	Br^-	-4.6	-5.1
	-	pyr-GBB (**5**)	O^-	-	-4.9	-5.5
	-	(**5**) - ester	-OEt	Br^-	-5.3	-6.1
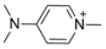	-	DMAP-GBB (**6**)	O^-	-	-5.0	-6.3
	-	**6** - ester	-OEt	Br^-	-5.0	-6.4
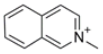	-	*i*-qui-GBB (**7**)	O^-	-	-6.0	-7.2
	-	**7** - ester	-OEt	Br^-	-6.0	-7.3
	-	qui-GBB (**8**)	O^-	-	-5.6	-6.7
	-	**8** - ester	-OEt	Br^-	-5.8	-6.8

Figure 2. Theoretically calculated affinity of the studied compounds.

The results show that, apart from Mildronate and MeGBB, all betaines exhibited stronger binding affinity than the natural substrate L-carnitine. Some aromatic compounds had similar values to their aliphatic analogs (e.g., pip-GBB vs. pyr-GBB, pyrr-GBB vs. mim-GBB), suggesting that additional π-π interaction may not significantly affect activity. A trend of increasing affinity with larger substituents indicated enhanced hydrophobic interactions (mim-GBB < pyr-GBB < DMAP-GBB < *i*-qui-GBB). Compounds **7** and **8**, with the most bulky substituents, isoquinoline and quinolone, respectively, showed the highest binding affinity with both enzymes. Unexpectedly, the ethyl ester salts gave results similar to their corresponding betaines, contrary to established experimental data (see below). Nevertheless, these theoretical calculations were regarded as a rational foundation for further experimental inquiry into the potential of these compounds as competitive inhibitors of CAT.

2.2. Synthesis and Characterization

The heterocyclic GBBs **1**-**8** were synthesized as per Scheme 1, following the procedure outlined by Tars and co-authors for preparing a wide range of acyclic aliphatic analogs of Meldonium (47). The synthetic pathway involves a quaternization reaction of a chosen amine with ethyl 4-bromobutanoate, followed by hydrolysis. In the alkylation step, acetonitrile was utilized as the reaction medium. Being a polar aprotic solvent, it stabilized the transition state by redistributing charges that appeared during the reaction while simultaneously preventing the inactivation of the starting amine. In the case of aliphatic amines, *N*,*N*-dimethyl-4-aminopyridine and *N*-methylimidazole, this first step proceeded with excellent yields (> 95%) under inert conditions at room temperature for 72 h. For isoquinoline and pyridine, the yields were notably lower (< 50%) the

 doi:10.20944/preprints202412.1211.v1

latter being attributed to their reduced nucleophilicity; therefore, their alkylation was accomplished at an elevated temperature of 40-80 °C with an extended reaction time (5-7 days), resulting in yields of 65-74%. The salts obtained in this manner were further hydrolyzed using a strongly basic ion exchange resin (Amberlite IRA-410(Cl)), and after neutralization, the final products were obtained by treatment with a strongly acidic ion exchange resin (Amberlite IR120, hydrogen form, strongly acidic). Notably, the reaction with the quinoline resulted in a complex mixture with no measurable formation of the corresponding GBB-ester. As a result, we did not synthesize compound **8**.

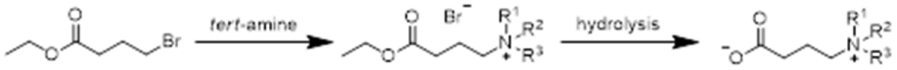

Scheme 1. Synthesis of heterocyclic gamma-butyrobetaines.

The so-outlined approach was not feasible for the conversion of 2-(4-ethoxy-4-oxobutyl)isoquinolin-2-yl bromide (**7**-ester) due to lower yields and the presence of additional impurities. Accordingly, 4-(isoquinolin-2-yl)butanoate (**7**) was synthesized by hydrolysis of **7**-ester in an acidic medium, subsequent neutralization with NaOH, conversion of the resulting NaBr and NaCl into their less soluble silver salts AgCl and AgBr, and the removal of the latter, as well as the additionally obtained $NaNO_3$, by precipitation in water and suitable organic solvents.

All synthesized compounds are highly hygroscopic, making their characterization and preparation of solutions for biological assessment challenging. The latter was resolved by utilizing ^{1}H-NMR spectroscopy with an internal standard of m-chlorobenzoic acid (m-CBA). Except for compounds **1**-ester, **3**, **3**-ester, **6** and **7**, literature data are available for the chemical shifts in the ^{1}H- and ^{13}C-NMR spectra, which are consistent with our results (47, 58-62). In the proton spectra of all compounds, with the exceptions of 4-(isoquinolin-2-yl)butanoate (**7**) and 4-(pyridin-1-yl)butanoate (**5**), distinct peaks can be observed, including a multiplet around 2.0 ppm corresponding to the two hydrogen atoms of the methylene group in the beta-position relative to the nitrogen atom, a triplet around 2.20 ppm for the two hydrogen atoms from the methylene group in the alpha- position relative to the carboxyl group (or ester), and a triplet in the range of 3.0-3.5 ppm for aliphatic amines (or 3.5-4.0 ppm for aromatics), corresponding to the methylene group attached to the quaternary nitrogen atom. Exception are compounds **5** and **7**, for which the latter signal is shifted beyond 4 ppm due to the nitrogen atom's substantial partial positive charge (a group with a positive mesomeric effect is missing).

2.3. Biological Assessment

To assess the impact of the synthesized compounds on CAT activity and establish the structure-activity relationship, we initially determined the concentration needed to reduce the enzyme activity by 50% (IC_{50}) under the same reaction conditions. We slightly modified a method proposed by Marquis and Fritz (63), which allows for the quantification of the consumed L-carnitine by observing its conversion to acetyl L-carnitine using a reaction with 5,5′-dithiobis-(2-nitrobenzoic acid) (DTNB or Ellman's reagent) and CoA to produce 2-nitro-5-thiobenzoic acid (TNB). We opted to determine the IC_{50} at a substrate concentration that yields a [S]/K_m ratio of about 0.01 (c(L-carnitine) = 50.56 uM and K_m = 3.0 mM) to ensure that the IC_{50} is virtually independent of [S]. We also used a kinetic approach, measuring the reaction rate over a time interval Δt, during which the dependence is linear (approximately 10-15% substrate conversion). The readings were taken within the first minute after the reaction began, and the degree of inhibition was determined as described in Section 3.3.1. The IC_{50} values for each compound were obtained by analyzing the percent inhibition at eight different inhibitor concentrations, with each measurement conducted in triplicate over three consecutive days. The average values of the IC_{50} obtained are outlined in Figure 3.

 doi:10.20944/preprints202412.1211.v1

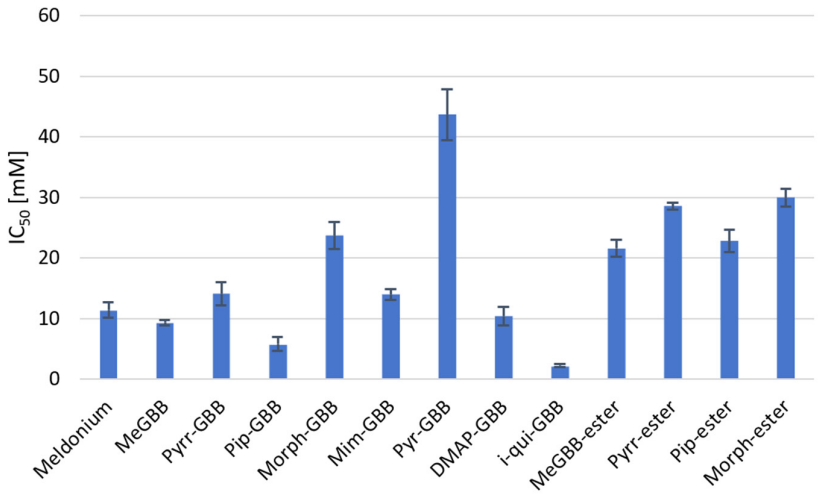

Figure 3. IC_{50} values of compounds **1**-**7**, four of the corresponding ethyl esters and the positive controls Meldonium and MeGBB.

Based on the results depicted in Figure 3, it is evident that all the compounds under investigation possess inhibitory efficacy within the low millimolar range (IC_{50} = 2.24-43.6 mM), with certain compounds demonstrating superior activity compared to the designated positive standards, Meldonium and MeGBB (IC_{50} = 11.4 ± 1.32 and 9.32 ± 0.47 mM, respectively). The exploration of structure-activity relationships allows for the formulation of the following general conclusions: (1) the volume of the gamma-position substituent has a direct impact on the affinity of the compounds being tested since it correlates directly with the observed inhibition capacity. In the case of aromatic derivatives, the activity increases in the order: Pyr-GBB < mim-GBB < DMAP-GBB < *i*-qui-GBB, aligning with the increasing size of the substituents. Additionally, the pyrrolidine derivative inhibitor (pyrr-GBB) demonstrated a significantly higher IC_{50} value (14.1 ± 1.91 mM) compared to its six-membered piperidine derivative (pip-GBB, IC_{50} = 5.8 ± 1.15 mM). This is further supported by the inhibitory capacity of the compound with the bulkiest isoquinolinium fragment (*i*-qui-GBB), showing the highest inhibitory capacity (IC_{50} = 2.24 ± 0.21 mM); (2) The presence of a free carboxyl group is essential for enhanced activity. This relationship is evident when comparing the activities of GBB compounds with their respective esters, wherein the IC_{50} values are observed to be twice as high for the esters; (3) increasing the polarity of the substituent in the gamma-position leads to a notable reduction in inhibitory ability. A comparison of the activity of *N*-methylmorpholine derivative (morph- GBB) with piperidine (pip-GBB) demonstrates this phenomenon. The presence of an oxygen atom in the morpholine ring increases the group's polarity in comparison to piperidine, thereby constraining the inhibitor's hydrophobic interactions within the enzyme's hydrophobic pocket; (4) the presence of an aromatic substituent in the gamma-position does not serve as a crucial determinant of heightened activity. This is evidenced by the fact that inhibitors featuring an aromatic substituent demonstrate comparable or decreased affinity compared to their aliphatic counterparts. Based on the dependencies derived in this manner, one can conclude that the presence of a free carboxyl group and a bulky non-polar substituent in the gamma-position is a prerequisite for more effective interaction of the inhibitors with the active center of the enzyme.

While IC_{50} values serve as informative indicators for comparative studies and SAR analyses, they do not provide a comprehensive understanding of the specific interactions between inhibitors and enzymes. Therefore, we performed a kinetic study of the most active compound, 4-(isoquinolin-2-yl)butanoate (**7**), to acquire more profound insights, as outlined in Section 3.3.2. Substrate concentrations were selected in the range of 0.2 to 5 times the K_m value (K_m = 0.3 mM) to facilitate effective inhibition detection at elevated levels while ensuring sufficient substrate availability for the reaction at increased inhibitor concentrations. Notably, higher inhibitor concentrations (7.5 mM and

 doi:10.20944/preprints202412.1211.v1

15 mM) resulted in deviations from the Michaelis-Menten model, so we worked at lower inhibitor concentrations (1.88 mM and 3.75 mM). Furthermore, at the lowest inhibitor concentration of 0.94 mM, the observed reaction rates were equivalent to those of blank samples, indicating a lack of inhibition; consequently, we excluded these values from subsequent analysis. The experiments enabled identification of the inhibition mechanism alongside calculations of K_m, V_{max}, and K_i. We utilized Sigma Plot version 12.5, which incorporates modules for regression analysis and various inhibition models. The numerical results are summarized in Table 2, while the corresponding Lineweavier-Burk and Michaelis-Menten kinetic plots are available in the Supplementary Materials. Our findings indicate that compound **7** functions as a competitive inhibitor of CAT, exhibiting a K_i value of 3.5 mM, which is comparable to that of the drug Mildronate (K_i = 1.63 mM). This finding suggests the potential role of compound **7** as a metabolic regulator within the human body.

Table 2. Coefficient of determination (R^2), Akaike Information Criterion (AIC) and Standard deviation of the residuals ($S_{y,x}$) for the different types of enzyme inhibition.

Type of inhibition	R^2	AIC	$S_{y.x}$
Competitive	0,99382	-1710,565	5.215e-9
Noncompetitive	0,97754	-1652,521	9.938e-9
Noncompetitive (partial)	0.97754	-1,649.983	1.006e-8
Uncompetitive	0,95923	-1625,683	1.339e-8
Uncompetitive (partial)	0.95922	-1,623.139	1.355e-8

3. Materials and Methods

3.1. General

All chemicals and CAT (isolated from pigeon breast muscle) used in this study were purchased from Sigma-Aldrich (FOT, Sofia, Bulgaria). The organic solvents were of analytical grade and were used without further purification. Molecular docking was performed with the freely available online platform Mcule (Mcule Inc, 535 Everett Ave 410 Palo Alto, CA 94301, USA; http://mcule.com). NMR spectra were recorded on a Bruker Avance III HD (500 MHz and 126 MHz for ^{1}H and ^{13}C, respectively) and Bruker Avance II+ (600 MHz and 151 MHz for ^{1}H and ^{13}C, respectively) using D_2O or $CDCl_3$ as a solvents. The chemicals shifts (δ) are given in ppm and J values are reported in Hz. Column chromatography was performed on Horizon High Performance FLASH chromatography system (HPFC) with cartridges filled with Silica gel 60 [particle size—0.06-0.2 mm (70-230 mesh), MACHEREY-NAGEL, Düren, Germany]. Biological assessment was performed on ELISA Reader Biotek 800TS (Biotek Instruments, Inc, ELTA90, Bulgaria). High-Resolution Mass Spectra (HRMS) were obtained on a Shimadzu LCMS-9050 (Shimadzu Handels GmbH., Korneuburg, Austria).

3.2. Synthesis

3.2.1. Synthesis of Bromide Salts of Heterocyclic Gamma-Butyrobetaine Ethyl Esters

The corresponding *tert*-amine (1.1 equiv.) was added to a solution of ethyl-4-bromobutanoate in acetonitrile and the resulting mixture was stirred under inert atmosphere (nitrogen) for 72 h. at r.t. (22-23° C), unless otherwise specified. At the end of the reaction, the unreacted amine and solvent were evaporated under reduced pressure, 250 mL of dry ethyl acetate were added to the residue and the mixture was cooled to 0° for 20 min. The resulting crystalline bromide salts of gamma-butyrobetaine ethyl esters were isolated after filtration.

4-ethoxy-*N*-ethyl-*N*,*N*-dimethyl-4-oxobutan-1-aminium bromide (MeGBB-ester). *N*,*N*-dimethylethylamine (2.53 g, 34.6 mmol) reacted with ethyl-4-bromobutanoate (6.13 g, 31.4 mmol) to give white crystals of MeGBB-ester (8.34 g, 99% yield), m.p. 108-110 ˚C (lit. 80.9-99.0 ˚C, [47]). ^{1}H-NMR (500 MHz, D_2O): δ = 4.24–4.17 (2H, m, O**CH**$_2$CH$_3$), 3.42 (2H, q, ^3J = 7.3 Hz, N**CH**$_2$CH$_3$), 3.38–3.28 (2H, m, 1-CH$_2$), 3.08 (6H, s, NCH$_3$), 2.53 (2H, t, ^3J = 7.0 Hz, 3-CH$_2$), 2.17–2.03 (2H, m, 2-CH$_2$), 1.36 (3H,

 doi:10.20944/preprints202412.1211.v1

t, ^3J = 7.2, NCH$_2$C**H**$_3$), 1.28 (3H, t, ^3J = 7.2 Hz, OCH$_2$C**H**$_3$). ^{13}C-NMR (126 MHz, D$_2$O): δ = 174.63 (C, C=O), 62.10, 61.98, 59.66, 50.06, 50.03, 50.00, 30.23, 17.42, 13.29, 7.41.

1-(4-ethoxy-4-oxobutyl)-1-methylpyrrolidin-1-ium bromide (Pyrr-ester, **1**–ester). *N*-methylpyrrolidine (2.73 g, 32.1 mmol) reacted with ethyl-4-bromobutanoate (5.69 g, 29.2 mmol) to give white crystals of Pyrr-ester (6.63 g, 81% yield), m.p. 117-119 ˚C (lit. 118-119 ˚C, [64]). ^{1}H-NMR (600 MHz, D$_2$O): δ = 4.15 (2H, q, ^3J = 7.2 Hz, OC**H**$_2$CH$_3$), 3.58–3.43 (4H, m, 2′-CH$_2$, 5′-CH$_2$), 3.40–3.31 (2H, m, 1-CH$_2$), 3.05 (3H, s, NCH3), 2.49 (2H, t, ^3J = 7.1 Hz, 3-CH$_2$), 2.24–2.15 (4H, m, 3′-CH$_2$, 4′-CH$_2$), 2.14–2.04 (2H, m, 2-CH$_2$), 1.24 (3H, t, ^3J = 7.2 Hz, OCH$_2$C**H**$_3$). ^{13}C-NMR (151 MHz, D$_2$O): δ = 174.77 (C=O), 64.49, 64.47, 64.45, 62.96, 62.05, 48.10, 30.46, 21.36, 18.72, 13.39.

1-(4-ethoxy-4-oxobutyl)-1-methylpiperidin-1-ium bromide (Pip-ester, **2**–ester). *N*-methylpiperidine (2.94 g, 29.7 mmol) reacted with ethyl-4-bromobutanoate (5.26 g, 27.0 mmol) to give white crystals of Pip-ester (7.55 g, 95% yield), m.p. 111-112 ˚C (lit. 112 ˚C, [65]). ^{1}H-NMR (600 MHz, D$_2$O) δ = 4.16 (2H, q, ^3J = 7.2 Hz, OC**H**$_2$CH$_3$), 3.38–3.30 (6H, m, 2′-CH$_2$, 6′-CH$_2$, 1-CH$_2$), 3.03 (3H, s, NCH$_3$), 2.48 (2H, t, ^3J = 7.0 Hz, 3-CH$_2$), 2.09–2.01 (2H, m, 2-CH$_2$), 1.88–1.83 (4H, m, 3′-CH$_2$, 5′-CH$_2$), 1.68–1.59 (2H, m, 4′-CH$_2$), 1.23 (3H, t, ^3J = 7.2Hz, OCH$_2$C**H**$_3$). ^{13}C-NMR (151 MHz, D$_2$O): δ = 174.77 (C=O), 62.06, 61.29, 30.37, 20.57, 19.57, 16.82, 13.38.

4-(4-ethoxy-4-oxobutyl)-4-methylmorpholin-4-ium bromide (Morph-ester, **3**–ester). *N*-methylmorpholine (2.97 g, 29.4 mmol)) reacted with ethyl-4-bromobutanoate (5.21 g, 26.7 mmol) to give white crystals of Morph-ester (4.82 g, 61% yield), m.p. 125-127 ˚C. ^{1}H-NMR (600 MHz, D$_2$O): δ = 4.20 (2H, q, ^3J = 7.2 Hz, OC**H**$_2$CH$_3$), 4.10–4.05 (4H, m, 3′-CH$_2$, 5′-CH$_2$), 3.61–3.51 (6H, m, 2′-CH$_2$, 6′-CH$_2$, 1-CH$_2$), 3.25 (3H, s, NCH$_3$), 2.56 (2H, t, ^3J = 7.0 Hz, 3-CH$_2$), 2.19–2.10 (2H, m, 2-CH$_2$), 1.30–1.26 (3H, t, ^3J = 7.2 Hz, OCH$_2$C**H**$_3$). ^{13}C-NMR (151 MHz, D$_2$O): δ = 174.59 (C=O), 62.09, 60.46, 59.72, 30.19, 16.64, 13.38. HRMS (ESI) m/z calculated for $[M]^+$ $C_{11}H_{22}NO_3^+$: 216.15942; found: $[M+H]^+$ 216.15921.

3.2.2. Synthesis of Heterocyclic Gamma-Butyrobetaines

The corresponding bromide salts of gamma-butyrobetaine ethyl esters obtained as describes in section 3.2.1. were dissolved in 3 mL dist. water and transferred to a column filled with strong base (Type II) anion exchange resin [Amberlite IRA-410(Cl), soaked in 10% (wt/wt) NaOH and washed with distilled water to pH = 7] in a ratio 1/10 (wt/wt). After 1h the column was eluted with dist. water and the pH of the resulting solution was adjusted with strong acid cation exchange resin (Amberlite IR120 H) to neutral value (pH = 7). The resin was then filtered, and, after evaporation of the filtrate, the residue was azeotropically dried with abs. ethanol to give the corresponding gamma-butyrobetaine. This procedure was used for the synthesis of all compounds except for *i*-qui-GBB, which was synthesized using a modified procedure.

4-(ethyldimethylammonio)butanoate (MeGBB). Isolated as yellow-brown oil (4.95 g, 99% yeld). ^{1}H-NMR (500 MHz, D$_2$O): δ = 3.41 (2H, q, ^3J = 7.3 Hz, NC**H**$_2$CH$_3$), 3.34–3.25 (2H, m, 4-CH$_2$), 3.07 (6H, s, NCH$_3$), 2.30 (2H, t, ^3J = 7.1 Hz, 2-CH$_2$), 2.08–1.96 (2H, m, 3-CH$_2$), 1.42–1.33 (3H, m, NCH$_2$C**H**$_3$). ^{13}C-NMR (126 MHz, D$_2$O): δ = 180.55 (C=O), 62.77, 59.65, 50.03, 50.00, 49.97, 33.33, 18.90, 7.43.

4-(1-methyl-1H-imidazol-3-ium-3-yl)butanoate (Mim-GBB, **4**). *N*-methylimidazole (2.67 g, 32.5 mmol) reacted with ethyl-4-bromobutanoate (5.76 g, 29.5 mmol) to white crystals of mim-ester (4.82 g, 61% yield), which, after hydrolysis give (4.57 g, 92%) yellow-brown oil of Mim-GBB. ^{1}H-NMR (500 MHz, D$_2$O): δ = 7.38–7.21 (2H, m, 4′-H, 5′-H), 4.02 (2H, t, ^3J = 7.1 Hz, 4-CH$_2$), 3.72 (3H, s, NCH$_3$), 2.06 (2H, t, ^3J = 7.3 Hz, 2-CH$_2$), 1.94 (2H, p, ^3J = 7.1 Hz, 3-CH$_2$). ^{13}C-NMR (126 MHz, D$_2$O): δ = 181.10 (C, C=O), 130.78, 123.46, 122.08, 48.94, 35.59, 33.73, 26.15.

4-(pyridin-1-ium-1-yl)butanoate (Pyr-GBB, **5**). Pyridine (2.62 g, 33.1 mmol) reacted with ethyl-4-bromobutanoate (5.87 g, 30.1mmol) at 40˚C for 5 days to white crystals of pyr-ester (3.80 g, 65% yield), which, after hydrolysis give Pyr-GBB as yellow-brown crystals (2.5 g, 50% yield), m.p. 63-65 ˚C (lit. 98-99 ˚C, [66]; 197-198 ˚C [58]). ^{1}H-NMR (500 MHz, D$_2$O): δ = 8.87 (2H, d, ^3J = 5.5 Hz, 2′-H, 6′-H), 8.59–8.52 (1H, m, 4′-H), 8.08 (1H, t, ^3J = 7.1 Hz, 3′-H, 5′-H), 4.66–4.61 (2H, m, 4-CH$_2$), 2.29–2.25 (4H, m, 3-CH$_2$, 2-CH$_2$). ^{13}C-NMR (126 MHz, D$_2$O): δ = 180.66 (C=O), 145.62, 144.30, 128.20, 61.39, 33.56, 27.34.

4-(4-(dimethylamino)pyridin-1-ium-1-yl)butanoate (DMAP-GBB, **6**). *N*,*N*-dimethyl-4-aminopyridine (9.62 g, 30.3 mmol) reacted with ethyl-4-bromobutanoate (5.38 g, 27.6 mmol) to white

 doi:10.20944/preprints202412.1211.v1

crystals of DMAP-ester (6.48 g, 99% yield), which, after hydrolysis give DMAP-GBB as yellow-brown oil (4.88 g, 98% yield). ^{1}H-NMR (500 MHz, D_2O): δ = 7.85 (2H, d, ^3J = 6.8 Hz, 2′-H, 6′-H), 6.67 (2H, d, ^3J = 6.8 Hz, 3′-H, 5′-H), 4.03 (2H, t, ^3J = 7.1 Hz, 4-CH_2), 3.05 (s, 6H; NCH_3), 2.15 (2H, t, ^3J = 7.3 Hz, 2-CH_2), 2.01 (2H, p, ^3J = 7.1 Hz, 3-CH_2). ^{13}C-NMR (126 MHz, D_2O): δ = 181.17 (C=O), 141.10, 107.41, 57.06, 39.24, 33.73, 26.90.

4-(isoquinolin-2-ium-2-yl)butanoate (*i*-qui-GBB, **7**). Isoquinoline (1 g, 7.74 mmol) reacted with ethyl-4-bromobutanoate (3.02 g, 15.48 mmol) at 80 °C for 7 days to give a complex oily mixture. The bromide salt of *i*-qui-GBB-ester was purified via flash chromatography (using MeOH as mobile phase), dissolved and stirred in 20 mL 2% HCl for 24 h. The resulting mixture was then neutralized with 10% NaOH, and 50% aqueous solution of $AgNO_3$ was added dropwise until no observable formation of AgCl or AgBr occurred. The inorganic salts were filtered, the solvent was evaporated under reduced pressure and abs. ethanol was added to the dry oily residue. The formed crystals of $NaNO_3$ were then filtered and the solvent was evaporated under reduced pressure to give *i*-qui-GBB (1.12 g, 67% yield), m.p. 149-152 °C. ^{1}H-NMR (600 MHz, $CDCl_3$): δ = 12.03 (1H, s, 1′-CH), 10.86 (1H, m, 3′-CH), 10.74–10.68 (2H, m, 4′-CH, 8′-CH), 10.55–10.50 (2H, m, 5′-CH, 6′-CH), 10.38–10.33 (1H, m, 7′-CH), 7.12 (2H, t, ^3J = 7.1 Hz, 4-CH_2), 4.74–4.68 (4H, m, 2-CH_2, 3-CH_2). ^{13}C-NMR (151 MHz, $CDCl_3$): δ = 183.13 (C=O), 151.57, 139.77, 139.44, 136.41, 133.74, 132.43, 129.93, 129.54, 128.86, 63.52, 36.11, 29.87. HRMS (ESI) m/z calculated for $[M+H]^+$ $C_{13}H_{13}NO_2$: 216.10191; found: $[M+H]^+$ 216.10170.

4-(1-methylpyrrolidin-1-ium-1-yl)butanoate (Pyrr-GBB, **1**). *N*-methylpyrrolidine (2.73 g, 32.1 mmol) reacted with ethyl-4-bromobutanoate (5.69 g, 29.2 mmol) to white crystals of pyrr-ester (6.63 g, 81% yield), which, after hydrolysis gives yellow-brown oil of Pyrr-GBB (4.05 g, 81% yield). ^{1}H-NMR (600 MHz, D_2O): δ = 3.51–3.38 (4H, m, 2′-CH_2, 5′- CH_2), 3.29–3.23 (2H, m, 4-CH_2), 2.99 (3H, s, NCH_3), 2.20 (2H, t, ^3J = 7.2 Hz, 2-CH_2), 2.18–2.10 (4H, m, 3′-CH2, 4′-CH2), 2.02–1.94 (2H, m, 3-CH_2). ^{13}C-NMR (151 MHz, D_2O): δ = 180.83 (C=O), 64.37, 64.35, 64.33, 63.60, 63.58, 48.04, 48.01, 47.99, 33.74, 21.30, 20.26.

4-(1-methylpiperidin-1-ium-1-yl)butanoate (Pip-GBB, **2**). *N*-methylpiperidine (2.94 g, 29.7 mmol) reacted with ethyl-4-bromobutanoate (5.26 g, 27.0 mmol) to white crystals of pip-ester (7.55 g, 95% yield), which, after hydrolysis gives yellow-brown oil of Pip-GBB (4.45 g, 89% yield). ^{1}H-NMR (600 MHz, D_2O): δ = 3.35–3.23 (6H, m, 2′-CH2, 6′-CH2, 4-CH_2), 2.99 (3H, s, NCH_3), 2.21 (2H, t, ^3J = 7.1 Hz, 2-CH_2), 1.98–1.90 (2H, m, 3-CH_2), 1.82 (4H, p, ^3J = 5.7 Hz, 3′-CH2, 5′-CH_2), 1.66–1.55 (2H, m, 4′-CH_2). ^{13}C-NMR (151 MHz, D_2O): δ = 180.87 (C=O), 62.54, 61.21, 47.85, 33.65, 20.59, 19.53, 18.33.

4-(4-methylmorpholino-4-ium)butanoate (Morph-GBB, **3**). *N*-methylmorpholine (2.97 g, 29.4 mmol) reacted with ethyl-4-bromobutanoate (5.21 g, 26.7 mmol) to white crystals of morph-ester (4.82 g, 61% yield), which, after hydrolysis gives yellow-brown oil of Morph-GBB (2.65 g, 53% yield). ^{1}H-NMR (600 MHz, D_2O): δ = 4.00 (4H, t, ^3J = 4.7 Hz, 3′-CH_2, 5′-CH_2), 3.52–3.39 (6H, m, 2′- CH_2, 6′- CH_2, 4-CH_2), 3.16 (3H, s, NCH_3), 2.23 (2H, t, ^3J = 7.1 Hz, 2-CH_2), 2.03–1.94 (2H, m, 3-CH_2). ^{13}C-NMR (151 MHz, D_2O): δ = 180.63 (C=O), 64.39, 60.43, 59.66, 46.94, 33.45, 18.16.

3.3. In-Vitro Studies

Carnitine acetyltransferase isolated from pigeon breast muscle, ammonium sulfate suspension, with activity 71 U/mg protein (1U converts 1 umol L-carnitine and 1 umol AcCoA in Acetylcarnitine and free CoA in 1 min) was diluted with phosphate buffer (pH = 7.6) to obtain stock solution with concentration 24 U/mL. Ellman reagent was freshly prepared just before use by dissolving 25 mg DTNB in 5 mL 1% Na_2EDTA aqueous solution in phosphate buffer (pH = 7.6). AcCoA, L-carnitine and each of the tested compounds were dissolved in distilled water in order to obtain desired stock solutions with concentration c (AcCoA) = 348.0 uM and c (L-carnitine) = 303.4 uM (for IC_{50} determination). Tris-buffer solution was prepared by dissolving Tris.HCl in distilled water and pH was adjusted with NaOH to pH = 7.6. The final volume of the reaction mixture was 300 uL, which includ 50 uL of each stock solution of CAT, AcCoA, L-carnitine, DTNB, Tris-buffer and test compound. In control probes, 50 uL distilled water was added instead of test compound. A mixture of CAT, AcCoA, DTNB, Tris-buffer and test compounds were incubated for 5 min at 37° C. The

 doi:10.20944/preprints202412.1211.v1

reaction was initiated by adding L-carnitine, and the reaction rate was monitored by measuring the absorbance at 405 nm.

3.3.1. IC_{50} Determination

Inhibition activity was assessed by calculating the reaction rate during the initial minute, within the linear range of A/t, utilizing the following formula:

$$\%Inh=100\times((\Delta A/\Delta t)control -(\Delta A/\Delta t)\ Inh)/((\Delta A/\Delta t)\ control)$$

To obtain preliminary data for the IC_{50} values, we initially screened each compound at a final concentration of 5 mM. Then, we prepared eight concentrations of each test compound, ranging from 20% to 80% of the IC_{50}, for further testing. The half-maximal inhibitory concentration (IC_{50}) was determined by plotting the response (A) against the concentration (c) of the inhibitor. All analyses were performed in triplicate over three consecutive days, and the corresponding IC_{50} values were averaged.

3.3.2. Enzyme Kinetics

The mechanism of inhibition for the most active compound was elucidated using five concentrations of the substrate, L-carnitine (ranging from 20% to 80% of K_m), and two concentrations of the inhibitor. For each substrate concentration, three separate reactions were performed: two with different concentrations of the inhibitor (1.88 mM and 3.75 mM) and one without it, the latter serving as a control. The absorbance at 405 nm was measured every 6 seconds between the 30th second and the 3rd minute for all probes (in the linear range). The initial velocity (v_0) was determined as the intercept of the velocity (v) versus time (t) graph. All experiments were conducted in triplicate over three consecutive days. Nonlinear regression analysis was performed using SigmaPlot, version 12.5. Graphical dependencies are provided in the Supplementary materials (Figure S1 and Figure S2).

4. Conclusions

Utilizing a combined approach of rational design, molecular docking, and in vitro studies, we showed the significant potential to serve as metabolic modulators for a series of heterocyclic analogs of gamma-butyrobetaine. These compounds exhibit the capability to regulate FAO through the inhibition of CAT, and perhaps other enzymes within the CT family. Comparative analysis has revealed that all compounds tested demonstrate inhibitory potential within the low millimolar region (IC_{50} = 2.24–43.6 mM), with some exhibiting greater activity than established standards such as Meldonium (marketed as Mildronate®, an approved drug for the treatment of heart ischemia, with IC_{50} = 11.39 ± 1.32 mM) and MeGBB (a drug candidate in phase III of clinical trials, with IC_{50} = 9.32 ± 0.47 mM). The determined IC_{50} values have facilitated additional insights into the structure-activity relationship: (1) the aromatic nature of the substituent in the gamma-position does not exert a significant influence on activity; (2) esterification of the carboxyl group, alongside an increase in the polarity of the substituent in the gamma position, markedly diminishes inhibitory ability; (3) the augmentation in the volume of substituents in the gamma-position correlates directly with the observed inhibition capacity. Further kinetic studies have identified the most active compound as a reversible competitive inhibitor of CAT with a K_i value of 3.5 mM, a level of inhibition comparable to the established drug Mildronate (K_i = 1.63 ± 0.52mM).

In conclusion, this study suggests the potential of the heterocyclic GBB analogs as agents for regulating metabolic processes in the human body and for treating ischemic disease, diabetes, and certain cancer types. Current experiments are being conducted to evaluate the toxicity and in vivo effects of selected compounds, and the results will be presented in due course.

Supplementary Materials: The following supporting information can be downloaded at the website of this paper posted on Preprints.org, Michaelis-Menten and Lineweaver-Burk plots for different types of inhibition; ^{1}H- and ^{13}C-NMR spectra of all compounds described in the script.

 doi:10.20944/preprints202412.1211.v1

Author Contributions: S.S. and M.G.B. contribute equally to this article. All authors have read and agreed to the published version of the manuscript.

Funding: This research received no external funding.

Data Availability Statement: The original contributions presented in this study are included in the supplementary material. Further inquiries can be directed to the corresponding author.

Conflicts of Interest: The authors declare no conflicts of interest.

References

1. Foley, J. Rationale and application of fatty acid oxidation inhibitors in treatment of diabetes mellitus. *Diabetes Care*. **1992**, *15*, 773-784.
2. Zhang, L.; Keung, W.; Samokhvalov, V.; Wang, W.; Lopaschuk, G. Role of fatty acid uptake and fatty acid beta-oxidation in mediating insulin resistance in heart and skeletal muscle. *Biochim. Biophys. Acta.* **2010**, *1801*, 1-22.
3. Hue, L.; Taegtmeyer, H. The Randle cycle revisited: a new head for an old hat. *Am. J. Physiol. Endocrinol. Metab.* **2009**, *297*, E578-591.
4. Ramsay, R.; Arduini, A. The carnitine acyltransferases and their role in modulating acyl-CoA pools. *Arch. Biochem. Biophys.* **1993**, *302*, 307-314.
5. Fritz, I.; Yue, K. Long-chain carnitine acyltransferase and the role of acylcarnitine derivatives in the catalytic increase of fatty acid oxidation induced by carnitine. *J. Lipid Res.* **1963**, *4*, 279-288.
6. Wang, M.; Wang, K.; Liao, X.; Hu, H.; Chen, L.; Meng, L.; Gao, W.; Li, Q. Carnitine Palmitoyltransferase System: A New Target for Anti-Inflammatory and Anticancer Therapy? *Front. Pharmacol.* **2021,** *12*, 760581.
7. Jacques, F.; Rippa, S.; Perrin, Y. Physiology of L-carnitine in plants in light of the knowledge in animals and microorganisms. *Plant. Sci.* **2018**, *274*, 432-440.
8. Govindasamy, L.; Kukar, T.; Lian, W.; Pedersen, B.; Gu, Y.; Agbandje-McKenna, M.; Jin, S.; McKenna, R.; Wu, D. Structural and mutational characterization of L-carnitine binding to human carnitine acetyltransferase. *J. Struct. Biol.* **2004**, *146*, 416-424.
9. Jogl, G.; Tong, L. Crystal structure of carnitine acetyltransferase and implications for the catalytic mechanism and fatty acid transport. *Cell.* **2003**, *112*, 113-122.
10. Bonnefont, J.; Djouadi, F.; Prip-Buus, C.; Gobin, S.; Munnich, A.; Bastin, J. Carnitine palmitoyltransferases 1 and 2: biochemical, molecular and medical aspects. *Mol. Aspects. Med.* **2004**, *25*, 495-520.
11. Sierra, A.; Gratacós, E.; Carrasco, P.; Clotet, J.; Ureña, J.; Serra, D.; Asins, G.; Hegardt, F.; Casals, N. CPT1c is localized in endoplasmic reticulum of neurons and has carnitine palmitoyltransferase activity. *J. Biol. Chem.* **2008**, *283*, 6878-6885.
12. Wu, D.; Govindasamy, L.; Lian, W.; Gu, Y.; Kukar, T.; Agbandje-McKenna, M.; McKenna, R. Structure of human carnitine acetyltransferase. Molecular basis for fatty acyl transfer. *J. Biol. Chem.* **2003**, *278*, 13159-13165.
13. Ramsay, R.; Gandour, R.; van der Leij, F. Molecular enzymology of carnitine transfer and transport. *Biochim. Biophys. Acta.* **2001**, *1546*, 21-43.
14. Randle, P.; Garland, P.; Hales, C.; Newsholme, E. The glucose fatty-acid cycle. Its role in insulin sensitivity and the metabolic disturbances of diabetes mellitus. *Lancet.* **1963**, *1*, 785-789.
15. Nechaeva, G.; Zheltikova, E. Effects of Meldonium in Early Postmyocardial Infarction Period. *Kardiologiia.* **2015**, *55*, 35-42.
16. Liamina, N.; Kotel'nikova, E.; Karpova, É.; Biziaeva, E.; Senchikhin, V.; Lipchanskaia, T. Cardioprotective capabilities of drug meldonium in secondary prevention after percutaneous coronary intervention in patients with documented myocardial ischemia. *Kardiologiia.* **2014**, *54*, 60-65.
17. Lopaschuk, G.; Wall, S.; Olley, P.; Davies, N. Etomoxir, a carnitine palmitoyltransferase I inhibitor, protects hearts from fatty acid-induced ischemic injury independent of changes in long chain acylcarnitine. *Circ. Res.* **1988**, *63*, 1036-1043.
18. Hübinger, A.; Knode, O.; Susanto, F.; Reinauer, H.; Gries, F. Effects of the carnitine-acyltransferase inhibitor etomoxir on insulin sensitivity, energy expenditure and substrate oxidation in NIDDM. *Horm. Metab. Res.* **1997**, *29*, 436-439.
19. Ratheiser, K.; Schneeweiss, B.; Waldhäusl, W.; Fasching, P.; Korn, A.; Nowotny, P.; Rohac, M.; Wolf, H. Inhibition by etomoxir of carnitine palmitoyltransferase I reduces hepatic glucose production and plasma lipids in non-insulin-dependent diabetes mellitus. *Metabolism.* **1991**, *40*, 1185-1190.
20. Liepinsh, E.; Vilskersts, R.; Zvejniece, L.; Svalbe, B.; Skapare, E.; Kuka, J.; Cirule, H.; Grinberga, S.; Kalvinsh, I.; Dambrova, M. Protective effects of mildronate in an experimental model of type 2 diabetes in Goto-Kakizaki rats. *Br. J. Pharmacol.* **2009**, *157*, 1549-1556.

 doi:10.20944/preprints202412.1211.v1

21. Liepinsh, E.; Skapare, E.; Svalbe, B.; Makrecka, M.; Cirule, H.; Dambrova, M. Anti-diabetic effects of mildronate alone or in combination with metformin in obese Zucker rats. *Eur. J. Pharmacol.* **2011**, *658*, 277-283.
22. Anderson, R. Carnitine Palmitoyltransferase: A Viable Target for the Treatment of NIDDM? *Curr. Pharm. Des.* **1998**, *4*, 1-15.
23. Giannessi, F.; Chiodi, P.; Marzi, M.; Minetti, P.; Pessotto, P.; De Angelis, F.; Tassoni, E.; Conti, R.; Giorgi, F.; Mabilia, M.; Dell'Uomo, N.; Muck, S.; Tinti, M.; Carminati, P.; Arduini, A. Reversible carnitine palmitoyltransferase inhibitors with broad chemical diversity as potential antidiabetic agents. *J. Med. Chem.* **2001**, *44*, 2383-2386.
24. Wagman, A.; Nuss, J. Current therapies and emerging targets for the treatment of diabetes. *Curr. Pharm. Des.* **2001,** *7*, 417-450.
25. Đurašević, S.; Stojković, M.; Bogdanović, L.; Pavlović, S.; Borković-Mitić, S.; Grigorov, I.; Bogojević, D.; Jasnić, N.; Tosti, T.; Đurović, S.; Đorđević, J.; Todorović, Z. The Effects of Meldonium on the Renal Acute Ischemia/Reperfusion Injury in Rats. *Int. J. Mol. Sci.* **2019**, *20*, 5747.
26. Đurašević, S.; Stojković, M.; Sopta, J. The effects of meldonium on the acute ischemia/reperfusion liver injury in rats. *Sci. Rep.* **2021**, *11*, 1305.
27. Mørkholt, A.; Wiborg, O.; Nieland, J. Blocking of carnitine palmitoyl transferase 1 potently reduces stress-induced depression in rat highlighting a pivotal role of lipid metabolism. *Sci. Rep.* **2017**, *7*, 2158.
28. Shriver, L.; Manchester, M. Inhibition of fatty acid metabolism ameliorates disease activity in an animal model of multiple sclerosis. *Sci. Rep.* **2011**, *1*, 79.
29. Mørkholt, A.; Oklinski, M.; Larsen, A.; Bockermann, R.; Issazadeh-Navikas, S.; Nieland, J.; Kwon, T.; Corthals, A.; Nielsen, S.; Nieland, J. Pharmacological inhibition of carnitine palmitoyl transferase 1 inhibits and reverses experimental autoimmune encephalitis in rodents. *PLoS One.* **2020**, *15*, e0234493.
30. Beitnere, U.; van Groen, T.; Kumar, A.; Jansone, B.; Klusa, V.; Kadish, I. Mildronate improves cognition and reduces amyloid-β pathology in transgenic Alzheimer's disease mice. *J. Neurosci. Res.* **2014**, *92*, 338-346.
31. Otsubo, C.; Bharathi, S.; Uppala, R.; Ilkayeva, O.; Wang, D.; McHugh, K.; Zou, Y.; Wang, J.; Alcorn, J.; Zuo, Y.; Hirschey, M.; Goetzman, E. Long-chain Acylcarnitines Reduce Lung Function by Inhibiting Pulmonary Surfactant. *J. Biol. Chem.* **2015**, *290*, 23897-23904.
32. Sainero-Alcolado, L.; Liaño-Pons, J.; Ruiz-Pérez, M.; Arsenian-Henriksson, M. Targeting mitochondrial metabolism for precision medicine in cancer. *Cell. Death. Differ.* **2022**, *29*, 1304–1317.
33. Melone, M.; Valentino, A.; Margarucci, S.; Galderisi, U.; Giordano, A.; Peluso, G.; The carnitine system and cancer metabolic plasticity. *Cell Death Dis.* **2018**, *9*, 228.
34. Samudio, I.; Harmancey, R.; Fiegl, M.; Kantarjian, H.; Konopleva, M.; Korchin, B.; Kaluarachchi, K.; Bornmann, W.; Duvvuri, S.; Taegtmeyer, H.; Andreeff, M. Pharmacologic inhibition of fatty acid oxidation sensitizes human leukemia cells to apoptosis induction. *J. Clin. Invest.* **2010**, *120*, 142-156.
35. Slebe, F.; Rojo, F.; Vinaixa, M.; García-Rocha, M.; Testoni, G.; Guiu, M.; Planet, E.; Samino, S.; Arenas, E.; Beltran, A.; Rovira, A.; Lluch, A.; Salvatella, X.; Yanes, O.; Albanell, J.; Guinovart, J.; Gomis, R. FoxA and LIPG endothelial lipase control the uptake of extracellular lipids for breast cancer growth. *Nat. Commun.* **2016**, *7*, 11199.
36. Kant, S.; Kesarwani, P.; Prabhu, A.; Graham, S.; Buelow, K.; Nakano, I.; Chinnaiyan, P. Enhanced fatty acid oxidation provides glioblastoma cells metabolic plasticity to accommodate to its dynamiC-Nutrient microenvironment. *Cell Death Dis.* **2020**, *11*, 253.
37. Ricciardi, M.; Mirabilii, S.; Allegretti, M.; Licchetta, R.; Calarco, A.; Torrisi, M.; Foà, R.; Nicolai, R.; Peluso, G.; Tafuri, A. Targeting the leukemia cell metabolism by the CPT1a inhibition: functional preclinical effects in leukemias. *Blood.* **2015**, *126*, 1925-1929.
38. Gugiatti, E.; Tenca, C.; Ravera, S.; Fabbi, M.; Ghiotto, F.; Mazzarello, A.; Bagnara, D.; Reverberi, D.; Zarcone, D.; Cutrona, G.; Ibatici, A.; Ciccone, E.; Darzynkiewicz, Z.; Fais, F.; Bruno, S. A reversible carnitine palmitoyltransferase (CPT1) inhibitor offsets the proliferation of chronic lymphocytic leukemia cells. *Haematol.* **2018**, *103*, 531-536.
39. Yao, C.; Liu, G.; Wang, R.; Moon, S.; Gross, R.; Patti, G. Identifying off-target effects of etomoxir reveals that carnitine palmitoyltransferase I is essential for cancer cell proliferation independent of β-oxidation. *PLoS Biol.* **2018**, *16*, 2003782.
40. Pacilli, A.; Calienni, M.; Margarucci, S.; D'Apolito, M.; Petillo, O.; Rocchi, L.; Pasquinelli, G.; Nicolai, R.; Koverech, A.; Calvani, M.; Peluso, G.; Montanaro, L. Carnitine-acyltransferase system inhibition, cancer cell death, and prevention of myc-induced lymphomagenesis. *J. Nat. Cancer Inst.* **2013**, *105*, 489-498.
41. Cheng, S.; Wang, G.; Wang, Y.; Cai, L.; Qian, K.; Ju, L.; Liu, X.; Xiao, Y.; Wang, X. Fatty acid oxidation inhibitor etomoxir suppresses tumor progression and induces cell cycle arrest via PPARγ-mediated pathway in bladder cancer. *Clin. Sci. (Lond).* **2019**, *133*, 1745-1758.
42. Simkhovich, B.; Shutenko, Z.; Meirena, D.; Khagi, K.; Mezapuķe, R.; Molodchina, T.; Kalviņs, I.; Lukevics, E. 3-(2,2,2-Trimethylhydrazinium)propionate (THP)—a novel gamma-butyrobetaine hydroxylase inhibitor with cardioprotective properties. *Biochem. Pharmacol.* **1988**, *37*, 195-202.

 doi:10.20944/preprints202412.1211.v1

43. Berlato, D.; Bairros, A. Meldonium: Pharmacological, toxicological and analytical aspects. *Toxicol. Res. Appl.* **2020**, *4*, 239784732091514.
44. Jaudzems, K.; Kuka, J.; Gutsaits, A.; Zinovjevs, K.; Kalvinsh, I.; Liepinsh, E.; Liepinsh, E.; Dambrova, M. Inhibition of carnitine acetyltransferase by mildronate, a regulator of energy metabolism. *J. Enzyme Inhib. Med. Chem.* **2009**, *24*, 1269-1275.
45. Kruszynska, Y.; Sherratt, H. Glucose kinetics during acute and chronic treatment of rats with 2[6(4-chlorophenoxy)hexyl]oxirane-2-carboxylate, etomoxir. *Biochem. Pharmacol.* **1987**, *36*, 3917-3921.
46. Gerondaes, P.; Alberti, K.; Agius, L. Interactions of inhibitors of carnitine palmitoyltransferase I and fibrates in cultured hepatocytes. *Biochem. J.* **1988**, *253*, 169-173.
47. Tars, K,; Leitans, J.; Kazaks, A.; Zelencova, D.; Liepinsh, E.; Kuka, J.; Makrecka, M.; Lola, D.; Andrianovs, V.; Gustina, D.; Grinberga, S.; Liepinsh, E.; Kalvinsh, I.; Dambrova, M.; Loza, E.; Pugovics, O. Targeting carnitine biosynthesis: discovery of new inhibitors against γ-butyrobetaine hydroxylase. *J. Med. Chem.* **2014**, *57*, 2213-2236.
48. Dambrova, M.; Makrecka-Kuka, M.; Vilskersts, R.; Makarova, E.; Kuka, J.; Liepinsh, E. Pharmacological effects of meldonium: Biochemical mechanisms and biomarkers of cardiometabolic activity. *Pharmacol. Res.* **2016**, *113*, 771-780.
49. Grube, M.; Meyer zu Schwabedissen, H.; Präger, D.; Haney, J.; Möritz, K.; Meissner, K.; Rosskopf, D.; Eckel, L.; Böhm, M.; Jedlitschky, G.; Kroemer, H. Uptake of cardiovascular drugs into the human heart: expression, regulation, and function of the carnitine transporter OCTN2 (SLC22A5). *Circulation.* **2006**, *113*, 1114-1122.
50. Schmitz, F.; Rösen, P.; Reinauer, H. Improvement of myocardial function and metabolism in diabetic rats by the carnitine palmitoyl transferase inhibitor Etomoxir. *Horm. Metab. Res.* **1995**, *27*, 515-522.
51. Morillas, M.; Clotet, J.; Rubí, B.; Serra, D.; Ariño, J.; Hegardt, F.; Asins, G. Inhibition by etomoxir of rat liver carnitine octanoyltransferase is produced through the co-ordinate interaction with two histidine residues. *Biochem. J.* **2000**, *351*, 495-502.
52. Lilly, K.; Chung, C.; Kerner, J.; VanRenterghem, R.; Bieber, L. Effect of etomoxiryl-CoA on different carnitine acyltransferases. *Biochem. Pharmacol.* **1992**, *43*, 353-61.
53. O'Connor, R.; Guo, L.; Ghassemi, S.; Snyder, N.; Worth, A.; Weng, L.; Kam, Y.; Philipson, B.; Trefely, S.; Nunez-Cruz, S.; Blair, I.; June, C.; Milone, M. The CPT1a inhibitor, etomoxir induces severe oxidative stress at commonly used concentrations. *Sci. Rep.* **2018**, *8*, 6289.
54. Holubarsch, C.; Rohrbach, M.; Karrasch, M.; Boehm, E.; Polonski, L.; Ponikowski, P.; Rhein, S. A double-blind randomized multicentre clinical trial to evaluate the efficacy and safety of two doses of etomoxir in comparison with placebo in patients with moderate congestive heart failure: the ERGO (etomoxir for the recovery of glucose oxidation) study. *Clin. Sci. (Lond.)* **2007**, *113*, 205-212.
55. Johnson, T.; Kocher, H.; Anderson, R.; Nemecek, G. Cloning, sequencing and heterologous expression of a cDNA encoding pigeon liver carnitine acetyltransferase. *Biochem. J.* **1995**, *305*, 439-444.
56. Chase, J. Carnitine acetyltransferase from pigeon breast muscle: [EC 2.3.1.7 Acetyl-CoA: carnitine O-acetyltransferase. **1969**, *13*, 387-393.
57. Mcule. Available online: http://mcule.com.
58. Szafran, M.; Dega-Szafran, Z.; Nowak-Wydra, B.; Pietrzak, M. Differences in proton–proton coupling constants of N+–CH2–CH2 protons of some betaines, N+–(CH2)2-3–COO–, and their complexes in aqueous solution. *J. Mol. Struct.* **2001**, *563–564*, 555-564.
59. Chevalier, A.; Zhang, Y.; Khdour, O.; Hecht, S. Selective Functionalization of Antimycin A Through an N-Transacylation Reaction. *Org. Lett.* **2016**, *18*, 2395-2398.
60. Kuroda, K.; Satria, H.; Miyamura, K.; Tsuge, Y.; Ninomiya, K.; Takahashi, K. Design of Wall-Destructive but Membrane-Compatible Solvents. *J. Am. Chem. Soc.* **2017**, *139*, 16052-16055.
61. Dega-Szafran, Z.; Dulewicz, E.; Szafran, M. 1H and 13C-NMR spectra of betaines, $>N^{+}(CH_2)_nCOO^{-}$, and their hydrogen halides. Additivity rules for carbon-13 chemical shifts. **2000**, *38*, 43-50.
62. Jadhav, S.; Ganvir, V.; Shinde, Y.; Revankar, S.; Thakre, S.; Singh, M. Carboxylate functionalized imidazolium-based zwitterions as benign and sustainable solvent for cellulose dissolution: Synthesis and characterization. *J. Mol. Liq.* **2021**, *344*, 117724.
63. Marquis, N.; Fritz, I. Enzymological determination of free carnitine concentrations in rat tissues. *J. Lipid. Res.* **1964**, *5*, 184–187.
64. Dega-Szafran, Z.; Przybylak, R. Synthesis, IR and NMR studies of zwitterionic ω-(1-pyrrolidine)alkanocarboxylic acids and their N-methyl derivatives. *J. Mol. Struct.* **1997**, *436-437*, 107-121.
65. Barczynski, P.; Dega-Szafran, Z.; Dulewicz, E.; Petryna, M. Aqueous basicity and proton affinity of zwitterionic omega-(N-methylpiperidine)-alkanocarboxylates and omega-(N-piperidine)-alkanocarboxylic acids. *Pol. J. Chem.* **2000**, *74*, 1149-1161.
66. Lukeš, R.; Pliml, J. Die reduktion von Pyridinbasen durch Ameisensäure VIII. Über die Reduktion von N-(Äthoxycarbonylalkyl)-pyridiniumformiaten. *Collect. Czech. Chem. Commun.* **1956**, *21*, 1602-1606.

 doi:10.20944/preprints202412.1211.v1